CHEMISTRY OF MATERIALS
Article

Chem. Mater. **2010,** *22,* 3079–3085 3079
DOI:10.1021/cm903780m

Exceptional Photocatalytic Activity of Ordered Mesoporous β-Bi_2O_3 Thin Films and Electrospun Nanofiber Mats

Kirstin Brezesinski,[†] Rainer Ostermann,[†] Pascal Hartmann,[†] Jan Perlich,[‡] and Torsten Brezesinski*[,†]

[†]*Institute of Physical Chemistry, Justus-Liebig-University Giessen, Heinrich-Buff-Ring 58, 35392 Giessen, Germany, and* [‡]*HASYLAB at DESY, Notkestrasse 85, 22603 Hamburg, Germany*

Received December 17, 2009. Revised Manuscript Received April 5, 2010

Herein, we report the synthesis and photocatalytic properties of novel Bi_2O_3 nanomaterials. Cubic mesoporous films were produced by coassembly of hydrated bismuth nitrate with a poly(ethylene-*co*-butylene)-*block*-poly(ethylene oxide) diblock copolymer, referred to as KLE, while nanofiber mats were produced via electrospinning. We establish that all materials employed in this work are highly crystalline after thermal treatment and that the nanoscale order of the self-assembled samples is further retained. KLE-templated films can readily produce phase-pure β-Bi_2O_3 with an optical band gap of about 3.4 eV. Calcination of nanofibers, by contrast, leads to the formation of a composite consisting of β-Bi_2O_3 and trace amounts of the thermodynamically stable α-Bi_2O_3 phase. We further show the benefits of a mesoporous morphology in heterogeneous semiconductor photocatalysis. KLE-templated β-Bi_2O_3 films exhibit much greater photocatalytic activity than nanofiber mats and nontemplated Bi_2O_3 films (prepared under otherwise identical conditions) as well as than KLE-templated anatase TiO_2 films on a mass normalized basis. We associate this exceptional activity with (1) the comparatively high BET surface area, which provides for a large number of adsorption sites, and (2) the high phase purity of the more catalytically active β-Bi_2O_3.

Introduction

Heterogeneous semiconductor photocatalysis has been the focus of much research due to potential applications of photoactive materials in the forefront field of environmental catalysis.[1−3] In recent years, it has been demonstrated that the photocatalytic activity strongly depends on (1) the ability of the catalyst to create electron−hole pairs, (2) recombination rates of electron−hole pairs both in the bulk and at the surface, which have been shown to be largely governed by atomic composition and population of structural defect sites, and (3) on the specific surface area of the photoactive material.

The search for oxides with tailored photocatalytic properties has been predominantly centered on the control of atomic structure, i.e., composition and defect structure. A wide variety of self-organization processes, however, now allows us to add a new variable to the arsenal of materials design, namely control over nanoscale structure. This control has already been shown to have a profound effect on material properties and performance.[4−6]

Surfactant/polymer templating is a powerful tool that has been widely used to produce inorganic materials with long-range periodicities reminiscent of liquid lyotropic phases.[7−9] The formation of these materials relies on the solution phase coassembly of inorganic reagents with structure-directing agents. The corresponding thin film materials can be achieved by the same coassembly methods but using an evaporation-induced self-assembly (EISA) process.[10,11]

A range of different metal oxides has been made so far. The use of EISA to produce bismuth oxide phases with both ordered nanoscale porosity and crystalline framework has not yet been reported though. Part of the reason for the absence of such materials is undoubtedly the fact that the majority of the polymers used to template materials do not allow the initially amorphous inorganic walls to be crystallized while retaining nanoscale order. Overall, it is important to note that the experience of the

*E-mail: torsten.brezesinski@phys.chemie.uni-giessen.de.

(1) Palmisano, G.; Augugliaro, V.; Pagliaro, M.; Palmisano, L. *Chem. Commun.* **2007**, *33*, 3425–3427.
(2) Carp, O.; Huisman, C. L.; Reller, A. *Prog. Solid State Ch.* **2004**, *32*, 33–177.
(3) Tryk, D. A.; Fujishima, A.; Honda, K. *Electrochim. Acta* **2000**, *45*, 2363–2376.
(4) Somorjai, G. A.; Frei, H.; Park, J. Y. *J. Am. Chem. Soc.* **2009**, *131*, 16589–16605.
(5) Ariga, K.; Vinu, A.; Hill., J. P.; Mori, T. *Coord. Chem. Rev.* **2007**, *251*, 2562–2591.
(6) Brezesinski, T.; Wang, J.; Tolbert, S. H.; Dunn, B. *Nat. Mater.* **2010**, *9*, 146–151.
(7) Beck, J. S.; Vartuli, J. C.; Roth, W. J.; Leonowicz, M. E.; Kresge, C. T.; Schmitt, K. D.; Chu, C. T. W.; Olson, D. H.; Sheppard, E. W.; McCullen, S. B.; Higgins, J. B.; Schlenker, J. L. *J. Am. Chem. Soc.* **1992**, *114*, 10834–10843.
(8) Goltner, C. G.; Antonietti, M. *Adv. Mater.* **1997**, *9*, 431–436.
(9) Sanchez, C.; Boissiere, C.; Grosso, D.; Laberty, C.; Nicole, L. *Chem. Mater.* **2008**, *20*, 682–737.
(10) Brinker, C. J.; Lu, Y. F.; Sellinger, A.; Fan, H. Y. *Adv. Mater.* **1999**, *11*, 579–585.
(11) Brezesinski, T.; Groenewolt, M.; Gibaud, A.; Pinna, N.; Antonietti, M.; Smarsly, B. M. *Adv. Mater.* **2006**, *18*, 2260–2263.

Published on Web 04/27/2010

past years has clearly shown that the synthesis of materials that combine key features like well-defined porosity, high crystallinity, and thermal stability still constitutes a major challenge to current templating routes. This work specifically focuses on bismuth trioxide (Bi_2O_3), a material that we show here how to synthesize with well-defined nanoscale porosity and highly crystalline walls.

Bismuth trioxide is the most significant compound of bismuth and is of potential interest for a wide range of applications including catalysis, gas sensing, and as the electrolyte in solid oxide fuel cells.[12−14] Bi_2O_3 is also known to have a large number of polymorphs, including the alpha (monoclinic), beta (tetragonal), gamma (body-centered cubic), delta (face-centered cubic), and omega (triclinic) phases. In recent years, however, only the beta and delta phases have attracted attention because of their interesting optical properties as well as high ionic conductivity at elevated temperatures.[15,16] In this context, it has been shown that β-Bi_2O_3 is also a feasible material for heterogeneous photocatalysis.[17−20] The preparation of purely tetragonal Bi_2O_3 is complicated, however, since the beta phase represents a metastable high temperature modification and is known to transform readily to α-Bi_2O_3. Creating Bi_2O_3 nanomaterials can be a viable solution to this problem because the interfacial energy of nanoscale materials is known to have a profound effect on both crystallization behavior and overall material stability. In addition, the catalytic properties can benefit from the typically high surface area of nanomaterials, which provides for a large number of adsorption sites.

In this work, we report the synthesis and photocatalytic properties of self-assembled films and electrospun fiber mats with nanocrystalline Bi_2O_3 domain structures. Through these experiments, the relationships among crystallite size, surface area, and catalytic activity are examined. We show that mesoporous β-Bi_2O_3 films exhibit both exceptional photocatalytic activity and excellent cycling characteristics. Overall, this work is an excellent test bed for determining how ordered nanoscale porosity can be used to enhance photocatalytic activity in Bi_2O_3 nanomaterials.

Experimental Section

Materials. $Bi(NO_3)_3 \cdot 5H_2O$ (99.9%), acetylacetone (99.5%), and 2-methoxyethanol (99.8%) were purchased from Sigma-Aldrich. Polyvinyl butyral (PVB, Mowital B 60 H) was donated by Kuraray Europe. $H[(CH_2CH_2)_{0.67}(CH_2CHCH_2CH_3)_{0.33}]_{89}(OCH_2CH_2)_{79}OH$, referred to as KLE, was used as the organic template.

Synthesis of Films. In a water-free container, 250 mg of $Bi(NO_3)_3 \cdot 5H_2O$ dissolved in 1.3 mL of 2-methoxyethanol are combined with 40 mg of KLE dissolved in 0.7 mL of MeOH. Thin films are produced via dip-coating on polar substrates, including (100)-oriented silicon wafer and fluorine-doped SnO_2 glass. Optimal conditions are given for 20% relative humidity and a constant withdrawal rate of 10 mm/s. For best results, the as-prepared films are heated to 250 °C using a 6 h ramp and aged at this temperature for 12 h. After this treatment, the samples are heated to 400 °C using a 15 min ramp followed by a 2 min soak.

Synthesis of Fibers. In a typical procedure, 800 mg of $Bi(NO_3)_3 \cdot 5H_2O$ dissolved in both 0.8 mL of acetylacetone and 1 mL of 2-methoxyethanol are combined with 1.6 g of polyvinyl butyral (10 wt %) in MeOH. Nanofibers are produced via electrospinning on (100)-oriented silicon wafer or aluminum foil. For best results, the as-prepared fibers are calcined using a 1.5 h ramp to 400 °C followed by a 30 min soak.

Characterization. Bright-field TEM and SEM images were taken with a CM30-ST microscope from Philips (acceleration voltage: 300 kV) and a LEO GEMINI 982 instrument (acceleration voltage: 5 kV), respectively. GISAXS data were collected at the German synchrotron radiation facility HASYLAB/DESY on beamline BW4 using a MarCCD area detector and a sample−detector distance of 1820 mm. Measurements were performed at different angles of grazing incidence, β, defined as the angle between the X-ray beam and the plane of the substrate. In addition, the use of 30 μm thick silicon wafers as substrates enabled small-angle X-ray scattering (SAXS) measurements to be performed in transmission geometry. Wide-angle X-ray diffraction (WAXD) measurements were carried out on an X'Pert PRO diffractometer from Panalytical instruments (Cu Kα radiation) utilizing a $\theta-2\theta$ geometry. XPS spectra were acquired on a Physical Electronics ESCA 5600 spectrometer with monochromatic Al Kα X-ray source (power: 200 W/14 kV) and multichannel detector OmniIV. The electron takeoff angle to the sample surface was adjusted to 45°. The adventitious hydrocarbon C1s signal at 284.6 eV was used as the energy reference to correct for charging. The film thickness was determined with an Alpha Step IQ Surface Profiler from KLA Tencor. Optical absorption measurements were carried out on a PERKIN ELMER Lambda 900 UV/vis/IR spectrophotometer. A substrate made from fused silica and an aluminum mirror served as the reference for transmission and reflection measurements, respectively. Electrospinning was carried out in a homemade setup consisting of a high-voltage power supply (Spellman CZE1000R) and syringe pump (KDS Scientific). The applied electrical field was ~1 kV/cm, and the distance from the needle tip to the collector was adjusted to 6 cm.

For photodegradation experiments, 20 mL of an aqueous solution of 10 μmol/L rhodamine B (RhB) was illuminated with a UV lamp (8 W, wavelength 254 nm, Benda NU-8 KL) in the presence of (1) 60 nm thick KLE-templated films with a total area of 7.1 cm^2, (2) 50 nm thick nontemplated films with a total area of 16 cm^2, and (3) 1.1 mg of nanofibers. A control experiment was conducted with 190 nm thick KLE-templated anatase TiO_2 films with a total area of 12.7 cm^2. The change in absorbance at 554 nm was monitored with a UVIKON XS spectrophotometer.

Results and Discussion

As mentioned above, the synthesis of ordered mesoporous β-Bi_2O_3 films has not yet been reported and so the

(12) Anderson, A. B.; Kim, Y. S.; Ewing, D. W.; Grasselli, R. K.; Tenhover, M. *Surf. Sci.* **1983**, *134*, 237–256.
(13) Cabot, A.; Marsal, A.; Arbiol, J.; Morante, J. R. *Sens. Act. B* **2004**, *99*, 74–89.
(14) Laurent, K.; Wang, G. Y.; Tusseau-Nenez, S.; Leprince-Wang, Y. *Solid State Ionics* **2008**, *178*, 1735–1739.
(15) Shuk, P.; Wiemhofer, H. D.; Guth, U.; Gopel, W.; Greenblatt, M. *Solid State Ionics* **1996**, *89*, 179–196.
(16) Kharton, V. V.; Marques, F. M. B.; Atkinson, A. *Solid State Ionics* **2004**, *174*, 135–149.
(17) Xiaohong, W.; Wei, Q.; Li, L.; Yun, G.; Zhaoyang, X. *Catal. Commun.* **2009**, *10*, 600–604.
(18) Wang, C.; Shao, C.; Wang, L.; Zhang, L.; Li, X.; Liu, Y. *J. Colloid Interface Sci.* **2009**, *333*, 242–248.
(19) Wang, Y.; Wen, Y. Y.; Ding, H. M.; Shan, Y. K. *J. Mater. Sci.* **2010**, *45*, 1385–1392.
(20) Xiaohong, W.; Wei, Q.; Weidong, H. *J. Mol. Catal. A* **2007**, *261*, 167–171.

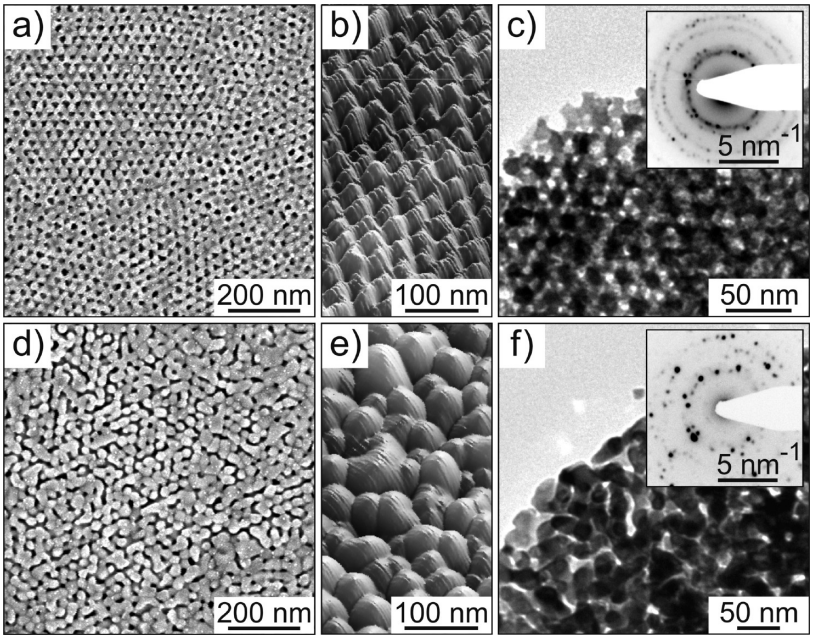

Figure 1. Morphology of KLE-templated β-Bi_2O_3 thin films heated to 400 °C (a−c) and 450 °C (d−f). (a and d) Top view SEM images. (b and e) 3D-AFM height images. The contrast covers height variations in the 1−6 nm (b) and 1−10 nm (e) range. (c and f) Bright-field TEM images. Electron diffraction patterns are shown in the insets.

ensuing section will focus on the characterization of these materials. In this work, we incorporated a poly(ethylene-*co*-butylene)-*block*-poly(ethylene oxide) diblock copolymer as the organic template (referred to as KLE), which has already been shown to be highly suitable for the direct synthesis of large-pore metal oxide films with nanocrystalline walls.[21−23] Part of the reason for this is that KLE polymers allow for the formation of cubic architectures with large domain structures and comparatively thick pore walls that can be crystallized readily. Moreover, they possess many desirable templating properties, such as high thermal stability and the ability to form ordered structures in a broad range of solvents.

Figures 1a−f and S1 (Supporting Information) show scanning electron microscope (SEM), tapping mode atomic force microscope (AFM), and bright-field transmission electron microscope (TEM) images of a KLE-templated β-Bi_2O_3 thin film heated to 400 (a−c) and 450 °C (d−f). Both top view SEM and AFM micrographs in Figure 1a and b reveal a well-defined cubic network of pores averaging 14−16 nm in diameter. It is evident from these images that the KLE-templated β-Bi_2O_3 films heated to 400 °C are crack-free and that the pores at the top surface are open. From TEM, we are able to establish that the periodic structure observed on the top surface persists throughout the film. The inset in Figure 1c is an electron diffraction pattern showing Debye−Scherrer rings characteristic of a material with randomly oriented nanocrystalline domains. Calculated lattice spacings are in perfect agreement with purely tetragonal Bi_2O_3.

Figures 1d−f show microscopy images of the same sample but after thermal treatment at 450 °C. It can be clearly observed that the film morphology changed. The in-plane pore ordering is clearly retained; however, the periodicity is significantly lower than that of films heated to 400 °C. The reason for the lack of long-range pore ordering can be attributed to sintering of crystallites in the pore walls into larger elongated crystals (Figure 1f). Also, the root-mean-square (rms) roughness of the top surface increased from 0.5 nm to ∼2 nm. Overall, however, the films are still crack-free and well-defined at atomic, mesoscopic, and macroscopic length scales.

By contrast, nanofiber mats were produced by electrospinning from a polyvinyl butyral (PVB) solution containing hydrated bismuth nitrate as the inorganic precursor.[24,25] Both SEM and TEM images in Figure 2 show nanocrystalline Bi_2O_3 fibers with widths of 90−110 nm and a few tens of micrometers in length. The width decreased from initially 250−300 nm (as-prepared) to ∼100 nm (at 400 °C) during thermal treatment. This shrinkage is due to combustion of both the nitrate ligands of the inorganic precursor and the carbon atoms of the PVB polymer present in the as-prepared composite fibers. We find that the morphology of the electrospun nanofibers shown in Figure 2 can be retained up to annealing temperatures of ∼450 °C (Supporting Information S1). Higher temperatures lead to strong restructurings, which we associate with the phase transformation of the β-Bi_2O_3 to

(21) Sallard, S.; Brezesinski, T.; Smarsly, B. M. *J. Phys. Chem. C* **2007**, *111*, 7200–7206.
(22) Brezesinski, T.; Smarsly, B.; Groenewolt, M.; Antonietti, M.; Grosso, D.; Boissière, C.; Sanchez, C. *Stud. Surf. Sci. Catal.* **2005**, *156*, 243–248.
(23) Richman, E. K.; Kang, C. B.; Brezesinski, T.; Tolbert, S. H. *Nano Lett.* **2008**, *8*, 3075–3079.
(24) Li, D.; Xia, Y. *Adv. Mater.* **2004**, *16*, 1151–1170.
(25) Greiner, A.; Wendorff, J. H. *Angew. Chem., Int. Ed.* **2007**, *46*, 5670–5703.

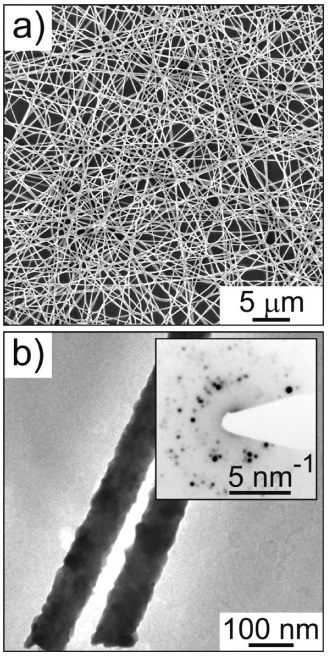

Figure 2. Morphology of electrospun α/β-Bi_2O_3 nanofibers calcined at 400 °C in air. (a) Low-magnification SEM image. (b) Bright-field TEM image. An electron diffraction pattern is shown in the inset of part b.

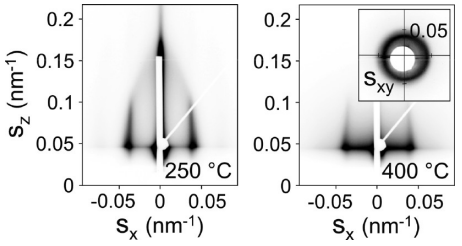

Figure 3. Synchrotron-based SAXS data obtained on ~150 nm thick KLE-templated Bi_2O_3 films heated to different annealing temperatures. GISAXS patterns were collected at an angle of incidence $\beta = 0.2°$ and show the evolution of the distorted cubic network of pores upon thermal treatment. A SAXS pattern taken in transmission mode is shown in the inset. Scattering vector, *s*, components are given in 1/nm.

the thermodynamically stable α-Bi_2O_3 phase. We note that similar observations have been made for other metal oxide nanofibers, such as VO_x.[26,27]

Structural characterization of the KLE-templated Bi_2O_3 materials is further supported by synchrotron-based grazing incidence small-angle X-ray scattering (GISAXS) data, which were collected at an angle of incidence $\beta = 0.2°$ at the German synchrotron radiation facility HASYLAB/DESY (see also 1D-SAXS in Bragg−Brentano geometry, Supporting Information S2).[28,29] Figure 3 shows GISAXS patterns obtained on ~150 nm thick films before and after the onset of crystallization. Samples with amorphous frameworks (250 °C/12 h) produce patterns with distinct off-specular and out-of-plane scattering maxima. These maxima can be indexed to a distorted cubic pore-solid architecture. Samples with crystalline framework (400 °C/2 min), by contrast, have lost their out-of-plane periodicity; the off-specular scattering maxima are still retained. The lack of out-of-plane periodicity, however, is a result of the small number of repeat units (about 9−11) normal to the plane of the substrate, and the fact that the crystallization of the initially amorphous material is always accompanied by a certain restructuring of the pore network. On the basis of the relative position of the out-of-plane reflection, a lattice contraction of more than 65% is determined for KLE-templated films calcined at 250 °C. The in-plane lattice contraction is negligible as the films are pinned to the substrate. We note that higher temperatures do not lead to further volume change as the self-assembled amorphous Bi_2O_3 materials are fully cross-linked after 12 h at 250 °C. The inset in Figure 3 is a SAXS pattern taken in transmission mode, i.e., at $\beta = 90°$. The presence of a distinct isotropic diffraction ring is typical of a material in which the in-plane pore ordering of the individual polycrystalline domains is in fact retained. Overall, the results with GISAXS and SAXS establish that the mesoporous morphology can be retained up to annealing temperatures of about 450 °C.

Porosity and Brunauer−Emmett−Teller (BET) surface area were determined by nitrogen physisorption experiments and weighing silicon substrates before and after film deposition. These measurements provide a BET surface area of 20−30 m^2/g, which is in good agreement with theoretical predictions for rather dense nanofibers. They also provide porosity values of 25−30% for mesoporous thin films calcined at 400 °C. With this value and the pore size obtained from both electron microscopy and X-ray scattering, a BET surface area of ~140 m^2/g is calculated assuming a low micropore fraction. We note that this value is characteristic of mesoporous materials templated with the diblock copolymer KLE.[6,30,31]

Lastly, a series of wide-angle X-ray diffraction (WAXD) and X-ray photoelectron spectroscopy (XPS) measurements were carried out to get insight into the crystallization behavior as well as to determine the elemental composition of the KLE-templated Bi_2O_3 materials. The crystalline nature appears to be important for the photocatalytic performance, and so, we examine the crystallization in detail in Figures 4a and S3 (Supporting Information). WAXD patterns obtained on thin films calcined at 400 °C demonstrate that these samples are composed of tetragonal Bi_2O_3 as corroborated with JCPDS reference card no. 27-0050. As neither WAXD nor electron diffraction indicates the presence of α-Bi_2O_3, we conclude that the amount of α-Bi_2O_3 in the KLE-templated samples employed in this work is negligible. We find, however, that annealing temperatures greater than ~450 °C lead to phase transformation and formation of secondary Bi_2O_3 phases (Supporting Information S3).

(26) Ostermann, R.; Li, D.; Yin, Y.; McCann, J. T.; Xia, Y. *Nano Lett.* **2006**, *6*, 1297–1302.
(27) Viswanathamurthi, P.; Bhattarai, N.; Kim, H. Y.; Lee, D. R. *Scripta Mater.* **2003**, *49*, 577–581.
(28) Muller-Buschbaum, P. *Anal. Bioanal. Chem.* **2003**, *376*, 3–10.
(29) Roth, S. V.; Dohrmann, R.; Dommach, M.; Kuhlmann, M.; Kroger, I.; Gehrke, R.; Walter, H.; Schroer, C.; Lengeler, B.; Muller-Buschbaum, P. *Rev. Sci. Instrum.* **2006**, *77*, 085106.
(30) Brezesinski, T.; Wang, J.; Polleux, J.; Dunn, B.; Tolbert, S. H. *J. Am. Chem. Soc.* **2009**, *131*, 1802–1809.
(31) Brezesinski, T.; Smarsly, B.; Iimura, K.; Grosso, D.; Amenitsch, H.; Antonietti, M.; Sanchez, C. *Small* **2005**, *1*, 889–898.

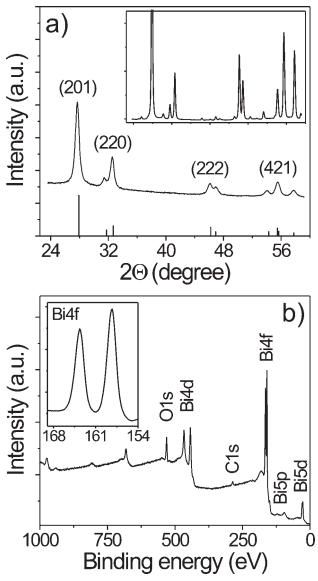

Figure 4. (a) Wide-angle XRD data obtained on a KLE-templated Bi_2O_3 thin film calcined at 400 °C. The stick pattern shows JCPDS reference card no. 27-0050 for tetragonal Bi_2O_3. A WAXD pattern obtained on electrospun Bi_2O_3 nanofiber mats calcined at 400 °C is shown in the inset of part a. Both diffractograms have the same scale on the *x*-axis for comparison. (b) Typical survey spectrum for KLE-templated β-Bi_2O_3 thin films. A high-resolution scan of the Bi4f region is shown in the inset of part b.

The crystallization of the initially amorphous films occurs within a narrow temperature interval (380−385 °C). Applying the Scherrer equation to the full width at half-maximum (FWHM) intensity of the (201) peak shown in Figure 4a provides an average crystallite size of 14 nm. The domain size in other crystallographic directions is only ∼11 nm, which implies the presence of slightly anisotropic crystallites in the pore walls. This result is not surprising, however, given the structural anisotropy of β-Bi_2O_3 (a = 7.742 Å, b = 7.742 Å, c = 5.631 Å). WAXD measurements further show that the FWHM intensity of the individual peaks does change with increasing annealing temperature (Supporting Information S3). Samples heated to 450 °C reveal a crystalline domain size of 23 nm × 18 nm, which is consistent with TEM results (Figure 1f). If the domain size of 11−14 nm is assumed to be the stable critical nucleation size, it helps explain why the same syntheses employed here failed when using other polymer templates, such as Pluronic F127 and P123, which generally achieve much smaller wall thicknesses.[23] The KLE diblock copolymer, in contrast, allows for the formation of sufficiently thick walls (10−20 nm depending on system) and, thus, also for the formation of stable nuclei/crystallites without the need to severely distort the pore network at the onset of crystallization.

The inset in Figure 4a shows a WAXD pattern obtained on nanofiber mats calcined at 400 °C. The crystallization occurs within a similar temperature interval. The average crystalline domain size, however, is significantly larger (∼35 nm) relative to KLE-templated films. This result is easy to understand and can be explained by the different impact of nanoconfinement on the crystallization behavior and crystal growth of Bi_2O_3. WAXD measurements on nanofiber mats also indicate trace amounts of the α-Bi_2O_3 phase, the formation of which could not be prevented by changing the heating profile.

Figure 4b shows a typical XPS survey scan for KLE-templated β-Bi_2O_3 thin films calcined at 400 °C. Aside from a weak C1s peak, only bismuth and oxygen core levels are observed, which confirms the absence of any contaminants. A closer examination of the C1s region shows that this peak can be associated with both adventitious carbon and partially combusted KLE template. The fact that the organic matter is not completely removed after heating films to 400 °C will become important in the following sections on photocatalytic activity.[31] Figure 4b further shows a high-resolution spectrum of the Bi4f region. The Bi4f level consists of a single doublet with binding energies of (163.64 ± 0.03) and (158.33 ± 0.03) eV for the f5/2 and f7/2 lines, respectively. Both peak position and separation (Δ = 5.31 eV) correspond well with reference data. For the same material, the atomic oxygen-to-bismuth ratio is found to be 1.54 ± 0.02. The deviation from perfectly stoichiometric Bi_2O_3 can be attributed to a small amount of extra oxygen at the film surface, presumably in the form of OH groups.

To examine the catalytic properties of Bi_2O_3, photodegradation experiments were conducted using rhodamine B (RhB) as the model pollutant. First, we determined the optical characteristics of the novel Bi_2O_3 nanomaterials using UV−vis spectroscopy. Absorbance spectra (data not shown) reveal only weak absorptions in the visible region of the electromagnetic spectrum although a few studies have shown that β-Bi_2O_3 is a potential new visible light responsive photocatalyst with a direct band gap smaller than 3.0 eV. In this regard, however, it is important to note that the reported measured values are highly inconsistent and range from 2.4 to 3.2 eV.[17,18,32−34]

For semiconductors with a direct band gap, the absorption coefficient, α, is proportional to the square root of the photon energy, $h\nu$, near the band gap energy, E_g, according to the following equation:

$$\alpha \propto (h\nu - E_g)^{1/2} \quad (1)$$

with $h\nu > E_g$. Figure 5a shows a plot of the square of the absorption coefficient as a function of photon energy for KLE-templated β-Bi_2O_3. It is evident from this data (see *x*-axis intercept point) that the optical band gap is ∼3.4 eV (equivalent to ∼360 nm light) for thin films calcined at 400 °C. The fact that this value differs from literature values for bulk β-Bi_2O_3 is not fully understood at this point but may be associated with slightly off-stoichiometry in our films and nanoconfinement effects (Laplace pressure, etc.). To verify the accuracy of this result, we also examined the photodegradation of RhB using 366 nm light as well as the wavelength-dependent photoelectrochemical methanol decomposition (Supporting Information S4). Both measurements

(32) Gujar, T. P.; Shinde, V. R.; Lokhande, C. D.; Mane, R. S.; Han, S.-H. *Appl. Surf. Sci.* **2005**, *250*, 161–167.
(33) Leontie, L.; Caraman, M.; Delibas, M.; Rusu, G. I. *Mater. Res. Bull.* **2001**, *36*, 1629–1637.
(34) Leontie, L.; Caraman, M.; Evtodiev, I.; Cuculescu, E.; Mija, A. *Phys. Stat. Sol.* (*a*) **2008**, *8*, 2052–2056.

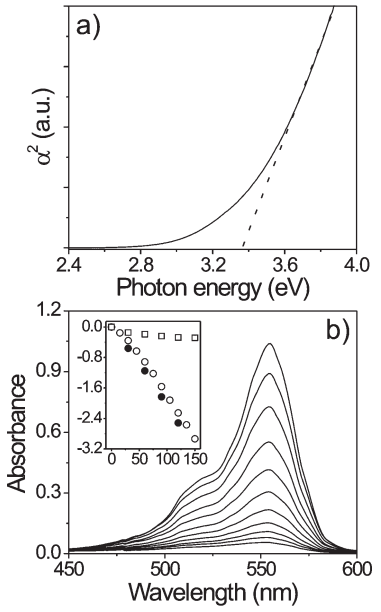

Figure 5. (a) Plot showing the square of the measured absorption coefficient as a function of photon energy. A band gap of ~3.4 eV is obtained for KLE-templated β-Bi_2O_3 calcined at 400 °C. (b) Photodegradation of RhB over an exposure period of 2.5 h (15 min steps) achieved by 60 nm thick KLE-templated β-Bi_2O_3 films. Semilogarithmic plots ($\ln(c/c_0)$ versus time) are shown in the inset of part b. Squares refer to the photodegradation of RhB in the absence of β-Bi_2O_3 while open and solid circles refer to the photodegradation in the presence of β-Bi_2O_3 after 1 and 3 cycles, respectively.

demonstrate that the β-Bi_2O_3 films employed in this work exhibit only low activity in the visible range. Thus, we decided to use 254 nm light to examine the catalytic properties.

The data shown in the ensuing section were obtained on 60 nm thick KLE-templated β-Bi_2O_3 films with a total area of 7.1 cm^2. Figure 5b shows UV−vis spectra collected at intervals of 15 min over an exposure period of 2.5 h. In addition, the inset in Figure 5b shows typical semilogarithmic plots for the photodegradation of RhB in the absence and presence of β-Bi_2O_3. It can be clearly seen that exposure of RhB to UV light does stimulate self-photodegradation. This pathway, however, is negligible when compared to the photodegradation achieved using KLE-templated β-Bi_2O_3 thin films. A closer examination of Figure 5b shows that the degradation kinetics are pseudo-first-order. The linear regression of data points obtained with β-Bi_2O_3 has a correlation constant of 0.995. At first glance, this high correlation constant implies that the linear regression is an excellent fit to the data. We find, however, that the slope determined by linear regression of the first two data points is quite different compared to that of the last nine ones. Removing the first two data points, i.e., those collected after exposure times of 0 and 15 min, results in a correlation constant of 0.999. This change seems minor but indicates different (slower) degradation kinetics within the first 15 min of the first cycle. We note that this result is always obtained for KLE-templated β-Bi_2O_3 films during the initial photodegradation cycle. The most plausible explanation is the presence of residual polymer template in the porous network blocking active sites upon the catalyst essential for the degradation of RhB. Upon removal of the remaining polymer, we find a steady increase in the degradation of RhB. The same samples also show excellent cycling characteristics as there is no decline in photocatalytic activity after three cycles. Moreover, the degradation rate is 3−4 times higher than that of the α/β-Bi_2O_3 nanofiber mats (Supporting Information S5) and even about 20 times higher compared to nontemplated films prepared under otherwise identical conditions (Supporting Information S1 and S6). Surprisingly, this correlates well with the difference in BET surface area. We thus associate the enhanced photocatalytic activity of the KLE-templated materials with the high density of accessible active sites offered by the mesoporous framework.

Lastly, a control experiment employing well-established KLE-templated anatase TiO_2 thin films as photocatalysts was conducted to ascertain the quality of catalysis achieved by the mesoporous β-Bi_2O_3 films.[30,31] The nanocrystalline titania frameworks are ideal candidates for comparison as they possess the same cubic architecture (Supporting Information S7) with similar BET surface area and optical band gap energy (Supporting Information S8) relative to KLE-templated β-Bi_2O_3 thin films.[30] Although TiO_2 is known to be a good photocatalyst,[35] we find a considerably lower degradation rate (about 10 times) on a mass normalized basis (Supporting Information S8), which underlines the exceptional photocatalytic properties of the novel β-Bi_2O_3 nanomaterials.

Conclusions

In summary, we have demonstrated that bismuth trioxide thin films can be templated using the amphiphilic diblock copolymer KLE. Moreover, we have also shown that nanofibers can readily be produced via electrospinning. The results with WAXD and GISAXS provide considerable insight on the structure of the self-assembled films and the crystallization process. KLE-templated samples can readily produce metastable β-Bi_2O_3 in phase-pure form, while thermal treatment of nanofiber mats leads to the formation of small amounts of the thermodynamically stable α-Bi_2O_3 phase. Although β-Bi_2O_3 has been proposed as a potential new visible light responsive material, we find a direct band gap of about 3.4 eV for films calcined at 400 °C.

The present work further establishes the benefits of a mesoporous morphology in heterogeneous photocatalysis. The catalytic activity of KLE-templated β-Bi_2O_3 thin films is significantly greater than that of nontemplated Bi_2O_3 thin films and KLE-templated anatase TiO_2 thin films. We attribute this exceptional activity both to the large BET surface area and to the high phase purity of the more catalytically active and robust nanocrystalline β-Bi_2O_3. A study of the influence of various dopants on the optical and

(35) Bian, Z. F.; Zhu, J.; Wang, S. H.; Cao, Y.; Qian, X. F.; Li, H. X. *J. Phys. Chem. C* **2008**, *112*, 6258–6262.

photocatalytic properties of mesoporous Bi_2O_3 is currently ongoing.

Acknowledgment. The authors thank Katarzyna Dudacy, Thomas E. Quickel, Anneliese Heilig, Stephan V. Roth, Bruno K. Meyer, and Ken-ichi Iimura for their assistance in materials preparation and characterization.

Supporting Information Available: Low-magnification SEM and TEM images. 1D-SAXS and temperature-dependent WAXD patterns. Photoelectrochemical experiments using KLE-templated Bi_2O_3 films. Photocatalytic experiments using (1) nontemplated Bi_2O_3 films, (2) Bi_2O_3 nanofibers, and (3) KLE-templated TiO_2 films. This material is available free of charge via the Internet at http://pubs.acs.org/.